Journal of Alloys and Compounds 506 (2010) 853–857

Contents lists available at ScienceDirect

Journal of Alloys and Compounds

journal homepage: www.elsevier.com/locate/jallcom

Effect of vanadium doping on the dielectric and nonlinear current–voltage characteristics of $CaCu_3Ti_4O_{12}$ ceramic

A. Sen [1], U.N. Maiti, R. Thapa, K.K. Chattopadhyay*

Thin Film and Nanoscience Laboratory, Department of Physics, Jadavpur University, Kolkata 700032, India

ARTICLE INFO

Article history:
Received 12 March 2010
Received in revised form 9 July 2010
Accepted 12 July 2010
Available online 18 July 2010

Keywords:
$CaCu_3Ti_4O_{12}$
Dielectric properties
Grain boundaries

ABSTRACT

Here we report the effect of vanadium doping on the dielectric and electrical properties of giant dielectric material $CaCu_3Ti_4O_{12}$ (CCTO), synthesized through conventional solid-state reaction process. Proper crystalline phase formation together with dopant induced lattice constant shrinkage was confirmed through X-ray diffraction studies. The X-ray photoelectron spectroscopic studies confirmed vanadium doping with V^{4+} replacing Ti^{4+} at its lattice site. The grain boundary resistivity was found to decrease monotonically with the increase of V doping percentages as revealed by impedance spectroscopic measurement and furthermore the grain size was found to follow the similar trend. The reduced grain boundary resistivity was found to be responsible for the overall variation of current density–electric field (J–E) characteristics.

1. Introduction

$CaCu_3Ti_4O_{12}$ (CCTO) has drawn much interest recently due to its extraordinarily high static dielectric constant (~10^4) which is practically frequency independent in the frequency range 10^2–10^6 Hz and possesses good temperature stability over a temperature range between 100 and 400 K [1–4]. However below 100 K, its dielectric constant drops dramatically to around 100. The unit cell of this titanate was identified as a body-centered cubic perovskite-like structure with Im3 space group and a lattice parameter of 7.391 Å. Until now, the origin of the giant dielectric response has not been fully understood. It is still questionable whether the high dielectric constant is intrinsic to a perfect crystal or extrinsic and related to the material microstructure (such as grain size) [5,6] and processing conditions (such as sintering temperature and time, cooling rate etc.) [7–11]. The most accepted mechanism till to date is an internal barrier layer capacitance (IBLC) model [12] in which the ceramic is supposed to consist of n-type semiconductive grains and insulating grain or domain boundaries [12–14].

Another physical feature in polycrystalline CCTO is its remarkable large electrostatic potential barrier that exists at the grain boundaries, as directly demonstrated by micro-contact current–voltage I–V measurements [15] and Kelvin probe force microscopy [16]. The presence of a potential barrier at grain boundaries along with the n-type semiconducting grains results in very strong nonlinear I–V characteristics, exhibiting the suppression of the current flow up to a threshold breakdown voltage. Based on the outstanding level of nonlinearity, a new application of CCTO as an efficient surge protector or as a switching device has been suggested by Chung et al. [15]. As the electrostatic potential at the grain boundaries can also be altered by the adsorption of selective gases, the resulting change in conductance can be monitored to detect the gases, as in other semiconductor-type gas sensors [17]. Furthermore, incorporating dopants into the CCTO can significantly alter the material behavior. In particular, transition metal doping in CCTO was found to influence the dielectric as well as their varistor properties [18–24]. The objective of the present investigation is to observe the effect of V substitution at the Ti site of the $CaCu_3Ti_4O_{12}$ ceramic and to monitor the changes in dielectric and nonlinear electric properties of the material.

2. Experimental procedures

Pure and V-doped CCTO ceramics were prepared by solid-state reaction of the reagent-grade chemicals, $CaCO_3$, CuO, and TiO_2, and V was substituted for Ti in the form of vanadium pentoxide (V_2O_5), which leads to the chemical formula $CaCu_3Ti_{4-x}V_xO_{12}$ (x = 0, 0.1, 0.3, 0.5 abbreviated as CCTVO_1, CCTVO_2, CCTVO_3 and CCTVO_4). Calculated quantities of $CaCO_3$, CuO, TiO_2 and V_2O_5 were mixed thoroughly with agate mortar and pestle using acetone as a solvent. The thoroughly mixed powders were then calcined at 1000 °C for 6 h with intermediate grinding and then furnace cooled. The fine powder of the compounds was pressed into pellets of 10 mm diameter and 1.5 mm thickness at a pressure of 5 MPa using a hydraulic press. The pellets were then sintered at 1040 °C for 10 h.

The prepared samples were studied with X-ray diffraction (XRD, Bruker, D-8 Advance) for structural investigation using the Cu K_α radiation of wavelength λ = 1.5406 Å. Composition analysis of the sample was done with X-ray photoemis-

* Corresponding author. Fax: +91 33 2414 6485.
E-mail addresses: kalyan_chattopadhyay@yahoo.com, kkc@juphys.ernet.in (K.K. Chattopadhyay).
[1] Present address: Department of Electronics, Bankura Christian College, West Bengal, India.

0925-8388/$ – see front matter © 2010 Elsevier B.V. All rights reserved.
doi:10.1016/j.jallcom.2010.07.094

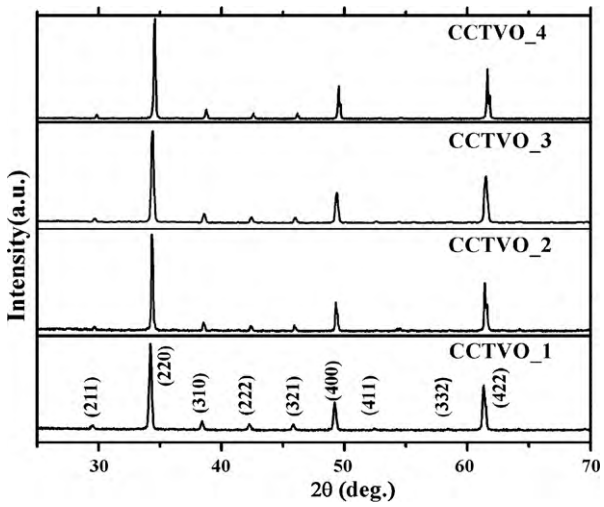

Fig. 1. XRD patterns of $CaCu_3Ti_{4-x}V_xO_{12}$ ceramics ($x = 0$, 0.1, 0.3, and 0.5) sintered at 1040 °C for 10 h.

sion spectroscopy (XPS SPECS, Germany) using Al K_α radiation as the X-ray source and the surface morphology of the sintered samples were carried out by a scanning electron microscope (SEM, JEOL-JSM-6360). For the dielectric measurements, Ag electrodes were screen printed with Ag pastes on both sides of the pellets and dielectric properties of pellets were measured using a HP 4284A precision LCR meter in the frequency range from 20 Hz to 1 MHz with applied ac voltage of 1 V at ambient temperature. The current–voltage (I–V) characteristics of the samples were studied using a Keithley 2410 source meter.

3. Results and discussion

The XRD patterns obtained for the pure and V-doped CCTO specimens are shown in Fig. 1. All the diffraction peaks appeared in the patterns matched with the peaks of the pseudo-cubic CCTO by comparing with the standard powder diffraction file database [JCPDF File No. 75-2188], with no traces from other impurity phases. However, compared with pure CCTO, minor shifts are observed in the peak positions for V-doped specimens.

The lattice parameter (as shown in Fig. 2) estimated from XRD patterns of pure CCTO were found to be 7.393 Å and is in close agreement with the other reported results [5]. The lattice parameter decreased with the increasing doping concentrations and it became 7.354 Å at $x = 0.5$. V^{4+} substitution at the Ti^{4+} site, as will be confirmed later through XPS analysis, causes this lattice constant

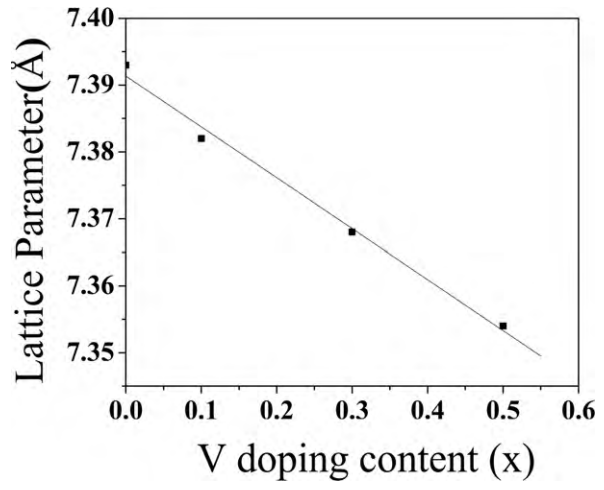

Fig. 2. Lattice parameters of $CaCu_3Ti_{4-x}V_xO_{12}$ ceramics ($x = 0$, 0.1, 0.3, and 0.5) as a function of vanadium substitution.

shrinkage due to difference in their ionic radius as reported to be 0.605 Å for Ti^{4+} whereas 0.59 Å for V^{4+} [25].

The XRD results allowed also determination of the crystallite sizes (D) of the samples. We use single-line analysis method to calculate the crystallite size for pure and doped samples. The full width at half maxima (FWHM) and integral breadth (β) were used for the single-line analysis method [26]. Integral breadth is mathematically expressed as the ratio of area under the curve and maximum height. In single-line analysis the Cauchy component of the Voigt function gives the value of crystallite size. The integral breadth of the Cauchy components of the profile (β_c) is given by the following empirical formula [26]:

$$\beta_c = \beta(a_0 + a_1\Phi + a_2\Phi^2) \quad (1)$$

where $\Phi = 2\omega/\beta$, $a_0 = 2.0207$, $a_1 = -0.4803$ and $a_2 = -1.7756$. The crystallite size of powder sample can be obtained from the relation:

$$D = \frac{\lambda}{(\beta_c \cos\theta)} \quad (2)$$

The FWHM, integral breadth, integral breadth of the Cauchy components and crystallite size derived from the XRD data are shown in Table 1. The reduction of crystal size with doping is mainly due to two reasons (i) difference between the ionic radii of the dopant atom with that of actual site atom and (ii) the increased defect density due to doping. These values show clearly that the doping process is responsible for a large decrease in the CCTO crystallite size with the increase of V substitution at the Ti site of the complex.

XPS survey scan for a V-doped CCTO sample is shown in Fig. 3(a). The spectrum is charge corrected with respect to adventitious C 1s peak at 284.6 eV. From the full XPS spectrum it is clear that only peaks corresponding to Ca, Cu, Ti and V appear which proves the compositional purity of the samples. Peaks due to Ca 2p3/2 and Cu 2p3/2 at 346.7 eV and 934.2 eV corresponds to pure CCTO sample [27]. High resolution XPS scan [Fig. 3(b)] in the energy interval 450–470 eV shows two prominent peaks with their positions at 458.3 eV and 463.17 eV which corresponds to the Ti 2p doublet namely Ti 2p3/2 and Ti 2p1/2 respectively. High resolution XPS spectra for V2p [Fig. 3(c)] also reveals similar type of doublet features with peaks at 516.3 eV and 523.57 eV associated with V 2p3/2 and V 2p1/2 respectively. Appearance of Ti 2p3/2 at 458.3 eV confirmed that Ti remains in the 4+ oxidation state within our CCTO crystals [27]. The V 2p3/2 in the 4+ oxidation state appeared at 516.2 eV [28], 516.3 eV [29], 515.7 eV [30] and 515.95 eV [31] where the same peak located at 517.11 eV [32,33], 516.95 eV [28] and 516.7 eV [34] when its oxidation state is 5+. For our CCTO sample, V 2p3/2 peak position was located in the energy range corresponding to 4+ oxidation state, thus we may conclude that V substituted Ti which remains in the 4+ oxidation state.

Fig. 4 shows the SEM microstructures and grain size distribution of CCTO ceramics with different V-dopant content. The morphology of the undoped sample is characterized by the grain size of the order of 5–30 μm with the bigger grains dominating the feature which decreases with increasing vanadium content. As x is reached up to 0.1 and 0.3, loosely linked grains having clear grain boundary with mean grain size ranging from 3 to 6 μm is observed with some holes. However, there is an indication of agglomeration (shown in inset) as V doping content is increased up to $x = 0.5$ with a further decrease in mean grain size. The influence of the above features has been visualized by monitoring the dielectric properties of various V-doped CCTO ceramics. The details of which are explained in the subsequent sections.

The frequency dependence of dielectric constant (ε_r) for undoped and V-doped CCTO ceramics at room temperature is shown in Fig. 5. All the samples show giant dielectric constant in a broad frequency range, which decreases gradually with increasing x. According to the internal boundary layer capaci-

Table 1
Crystallite size derived from single-line analysis of XRD profiles.

Sample name	$2\theta^\circ$	2ω	β	$\Phi = 2\omega/\beta$	β_c	D (nm)
$CaCu_3Ti_4O_{12}$	34.22	0.23	0.2560	0.8984	0.0399	403.9
$CaCu_3Ti_{3.9}V_{0.1}O_{12}$	34.33	0.17	0.1456	0.8642	0.0549	293.7
$CaCu_3Ti_{3.7}V_{0.3}O_{12}$	34.39	0.24	0.2803	0.8633	0.0792	203.6
$CaCu_3Ti_{3.5}V_{0.5}O_{12}$	34.57	0.13	0.1857	0.7005	0.1509	106.9

2ω: FWHM; β: measured integral breadth of observed profile; β_c: the integral breadth of the Cauchy components of the observed profile.

tance (IBLC) model, the "effective" permittivity can be estimated as $\varepsilon_{eff} = \varepsilon_{gb}(t_b/t_{gb})$ [6,35,36], where ε_{gb} is the permittivity of the insulating grain boundary phase, t_b the average grain size and t_{gb} the average grain boundary thickness. ε_{gb} was reported to vary with the extent of segregated phase at the grain boundary in case of CCTO [37,38]. We have investigated for the possible phase segregation at the grain boundary through EDX analysis which indicated compositional uniformity (within EDX detection limit) over the grain as well as the grain boundary. The effective dielectric constant (ε_{eff}) is inversely proportional to the ratio of thickness of the insulating layer (i.e. grain boundary) (t_{gb}) to the grain size (t_g) as expressed $\varepsilon_{eff} \sim 1/(t_{gb}/t_g)$, assuming that the dielectric constants for the grain and grain boundary are the same and the resistivity of grain boundary is much larger than that of the grain. Based on the above argument, the observed reduced dielectric constant for the small-grained V-substituted specimen may arise due to the change in the grain boundary thickness (or due to increase of the thickness ratio).

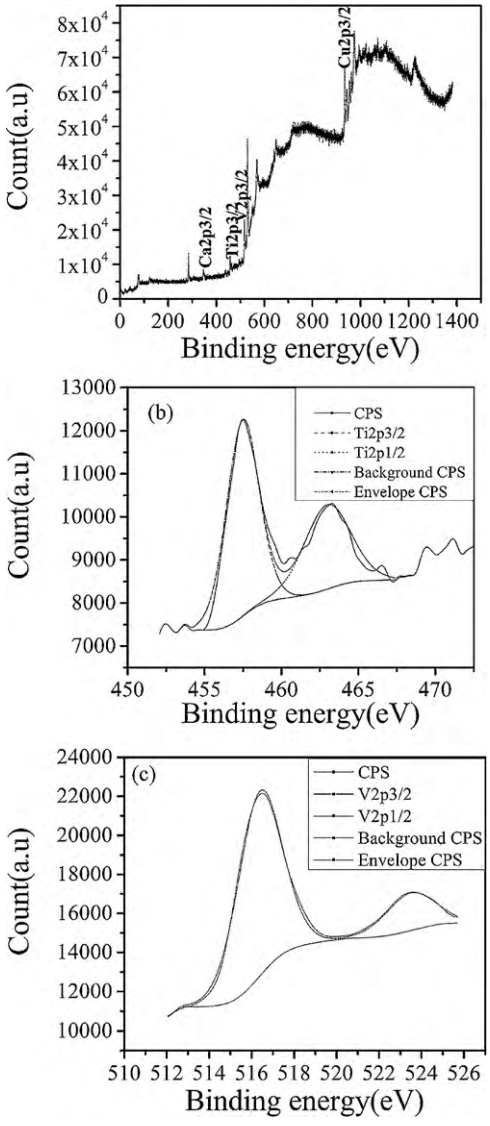

Fig. 3. (a) XPS survey scan for the sample $CaC_3Ti_{3.5}V_{0.5}O_{12}$. (b) High resolution XPS spectra for Ti 2p. (c) High resolution XPS spectra for V 2p.

As we know, the IBLC structure has an equivalent circuit consisting of two parallel RC elements connected in series. One parallel RC unit corresponds to the semiconducting grains/subgrains, (R_g, C_g) and another one (R_{gb}, C_{gb}), is for the insulating barrier layers. So one can easily write the expression of the total complex impedance as [39]:

$$Z(\omega) = \left(\frac{1}{R_g} + j\omega C_g\right)^{-1} + \left(\frac{1}{R_{gb}} + j\omega C_{gb}\right)^{-1}$$

The R_g and R_{gb} values can be obtained by impedance spectrum analysis. As shown in Fig. 6 the non-zero intercept on the Z' axis gives the R_g value and the R_{gb} value may also be directly obtained by the other intercept on the Z' axis from the low-frequency impedance data. However, the experimental impedance data around room temperature only cover a part of the semicircles or arcs because of the limit of the measured frequency range. In order to obtain a definite R_g value, we have made a data fitting and extrapolation using the Cole–Cole empirical relation. It can be seen that the addition of V has influence on the resistivity of the grain (R_g) and grain boundary (R_{gb}), especially for the grain boundary (see Table 2). With increasing doping, the V concentration obviously increased at the grain and grain boundaries with respect to the samples having lower doping concentration. Hence the grain boundary resistivity decreased with increase of V doping.

In addition to the dielectric properties, we also investigated the current–voltage characteristics of V-substituted samples. The current density–electric field (J–E) curves of the V-doped CCTO specimens are shown in Fig. 7. In general, the correlation between current and voltage for a varistor can be expressed by [40]

$$I = KV^{\alpha} \quad (3)$$

where K is a constant related to the electrical resistivity of the material and α is the nonlinear coefficient. As shown in the figure, a strongly nonlinear relationship is observed, clearly marking the breakdown voltages above which the current abruptly begins to flow. As more dopants are added, the threshold electric field decreases and the nonlinear coefficient also follow such trend. The breakdown voltage gradient is defined as the electric field intensity at 10 mA/cm^2 in this experiment. According to Eq. (3), the fitted J–E results show that the breakdown voltages of the samples

Table 2
The obtained values of R_g and R_{gb} from the fitting of complex impedance plot shown in Fig. 6.

Sample name	R_g (Ω cm)	R_{gb} (MΩ cm)
$CaCu_3Ti_4O_{12}$	56	–
$CaCu_3Ti_{3.9}V_{0.1}O_{12}$	170	1.14
$CaCu_3Ti_{3.7}V_{0.3}O_{12}$	147	0.41
$CaCu_3Ti_{3.5}V_{0.5}O_{12}$	142	0.31

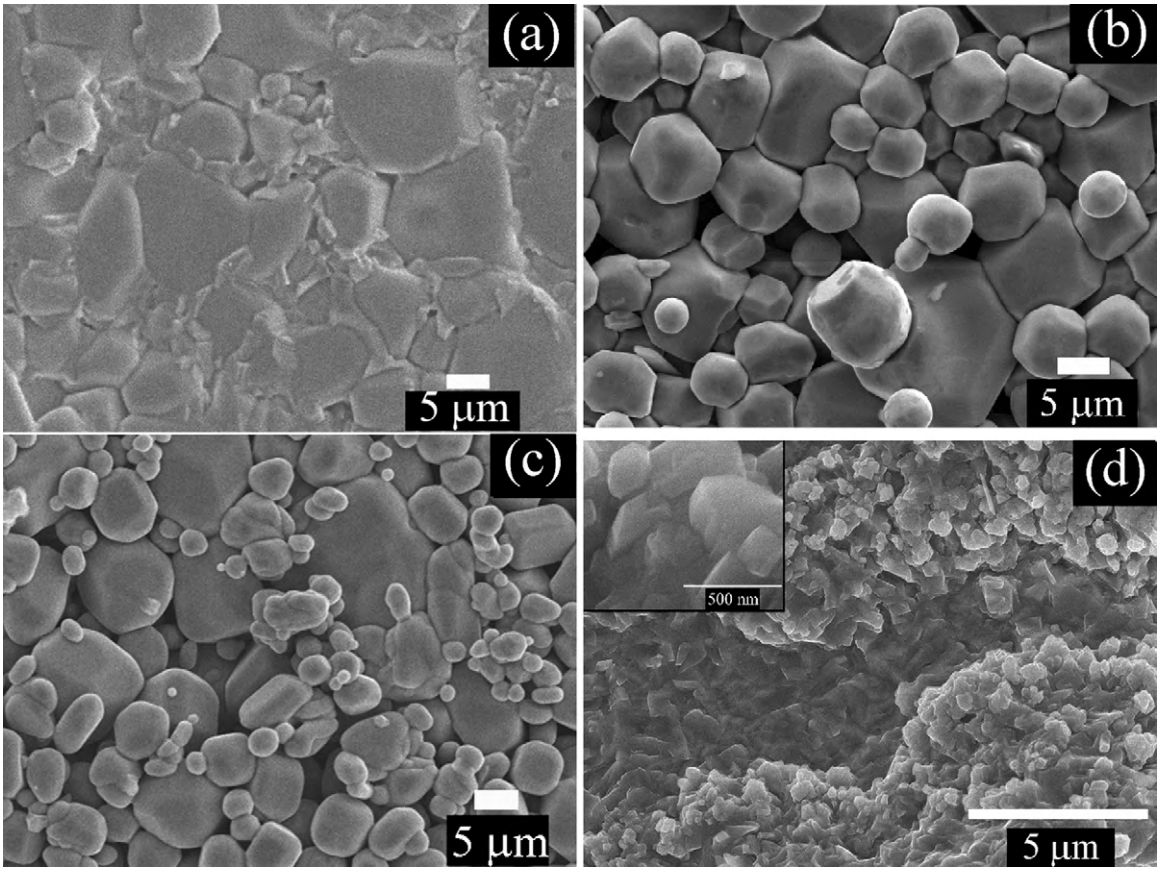

Fig. 4. The SEM images of $CaCu_3Ti_{4-x}V_xO_{12}$ ceramics (a) $x = 0$, (b) $x = 0.1$, (c) $x = 0.3$ and (d) $x = 0.5$ sintered at 1040 °C for 10 h.

are 442 V cm^{-1}, 185 V cm^{-1}, 101 V cm^{-1}, 26 V cm^{-1} and nonlinear coefficients are 37.57, 23.22, 6.15 and 1.65 for $x = 0$, 0.1, 0.3 and 0.5 respectively, which imply that the V doping can tune current voltage characteristics from non-ohmic to nearly ohmic nature. Therefore, it is shown that the threshold voltage can be easily controlled in a simple manner by V doping. The dopant induced change in breakdown phenomenon was explained here on the basis of impedance spectroscopy. The range of the nonlinear coefficient (α) values depend on the particular applications. Generally, for low voltage application, the value of alpha lies in the range 1.2–13 [41] and for high voltage application, it remains in the range 65–900 [16,42]. Thus the obtained (α) value indicates the applicability of the varistor in the mid voltage range.

High frequency resistance of the bulk grains as estimated from the first intercept of the characteristic semicircles in the impedance spectroscopy varies only slightly with increase of doping percentage. However, the diameter of the semicircular arc, which corresponds to the grain boundary resistance, is considerably reduced with V doping. From Table 2 it is clearly observed that the grain boundary resistivity decreased with increase of V doping. From Fig. 7, it can be observed that the break down occurred at

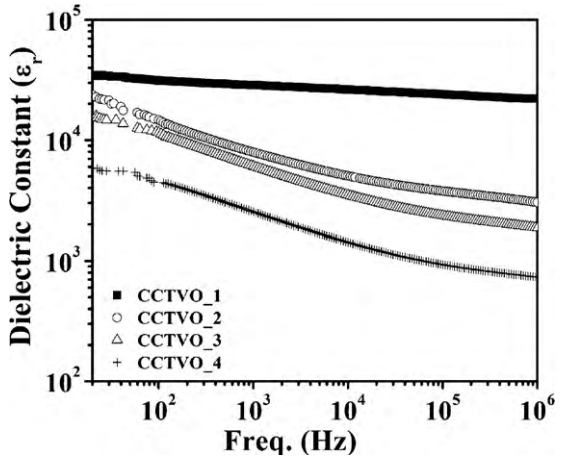

Fig. 5. Frequency dependence of dielectric constant of pure and vanadium doped $CaCu_3Ti_{4-x}V_xO_{12}$ ceramics measured at room temperature.

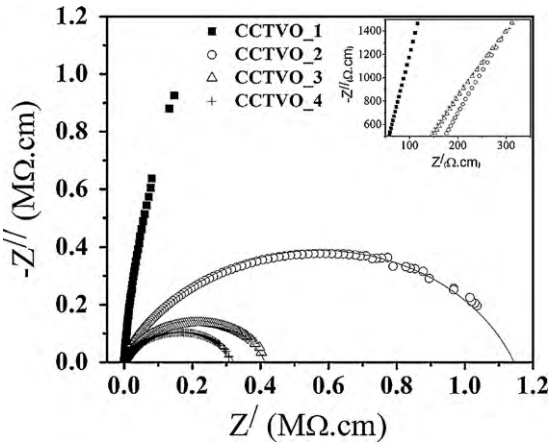

Fig. 6. Impedance complex plane plots for the vanadium doped $CaCu_3Ti_{4-x}V_xO_{12}$ ceramics at room temperature.

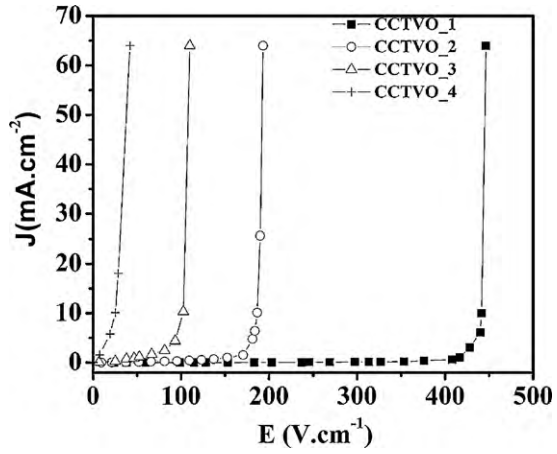

Fig. 7. Current density (J)–electric field (E) curves of various vanadium doped $CaCu_3Ti_{4-x}V_xO_{12}$ specimens at room temperature.

lower fields with increasing V doping. As ε_{gb} was assumed to be constant hence, the change in grain boundary resistivity must be the primary cause for lowering the break down field with increasing V doping.

4. Conclusions

In conclusion, influence of vanadium doping on the electric and dielectric properties of giant dielectric material CCTO was investigated. From the XPS studies it was confirmed that V^{4+} was substituted at the site of Ti^{4+}. The signature of vanadium doping was also observed in the grain size lowering of the CCTO ceramics which is one of the major factors in the variation in dielectric properties. The observed variations in the current density–electric field characteristics were found to be associated mainly with the change in the grain boundaries resistivities due to vanadium incorporation at the Ti site. In this regard, the present study may open up the possibility for the development of ceramic varistors with tunable breakdown voltage by changing the V doping percentages.

Acknowledgements

One of us (AS) wishes to thank Dr. Richard Rabindranath Bajpai, Principal, and Dr. D. Biswas, Bankura Christian College, for their valuable suggestions during the execution of the work. The authors wish to gratefully acknowledge the University Grants Commission (UGC), the Government of India, for financial assistance under 'The University with potential for excellence' scheme.

References

[1] C. Kant, T. Rudolf, F. Mayr, S. Krohns, P. Lunkenheimer, S.G. Ebbinghaus, A. Loidl, Phys. Rev. B 77 (2008) 045131–045137.
[2] L. Liu, H. Fan, X. Chen, P. Fang, J. Alloys Compd. 469 (2009) 529–534.
[3] C.C. Homes, T. Vogt, S.M. Shapiro, S. Wakimoto, A.P. Ramirez, Science 293 (2001) 673–676.
[4] M.A. Subramanian, A.W. Sleight, Solid State Sci. 4 (2002) 347–351.
[5] T. Li, Z. Chen, Y. Su, L. Su, J. Zhang, J. Mater. Sci. 44 (2009) 6149–6154.
[6] V. Brizé, G. Gruener, J. Wolfman, K. Fatyeyeva, M. Tabellout, M. Gervais, F. Gervais, Mater. Sci. Eng. B 129 (2006) 135–138.
[7] B.A. Bender, M.-J. Pan, Mater. Sci. Eng. B 117 (2005) 339–347.
[8] S. Kwon, D.P. Cann, J. Electroceram. 24 (2010) 231–236.
[9] J.J. Romero, P. Leret, F.R. Marcos, A. Quesada, J.F. Fernández, J. Eur. Ceram. Soc. 30 (2010) 737–742.
[10] B.S. Prakash, K.B.R. Varma, Physica B 403 (2008) 2246–2254.
[11] C.-M. Wang, S.-Y. Lin, K.-S. Kao, Y.-C. Chen, S.-C. Weng, J. Alloys Compd. 491 (2010) 423–430.
[12] D.C. Sinclair, T.B. Adams, F.D. Morrison, A.R. West, Appl. Phys. Lett. 80 (2002) 2153.
[13] L. Liu, H. Fan, P. Fang, X. Chen, Mater. Res. Bull. 43 (2008) 1800–1807.
[14] T.T. Fang, C.P. Liu, Chem. Mater. 17 (2005) 5167–5171.
[15] S.-Y. Chung, J.-H. Choi, J.-K. Choi, Appl. Phys. Lett. 91 (9) (2007) 091912.
[16] S.-Y. Chung, I.-D. Kim, S.-J.L. Kang, Nat. Mater. 3 (2004) 774–778.
[17] A. Rothschild, H.L. Tuller, J. Electroceram. 17 (2006) 1005–1012.
[18] L. Ramajo, R. Parra, J.A. Varela, M.M. Reboredo, M.A. Ramírez, M.S. Castro, J. Alloys Compd. 497 (2010) 349–353.
[19] S.-Y. Chung, S.-Y. Choi, T. Yamamoto, Y. Ikuhara, S.-J.L. Kang, Appl. Phys. Lett. 88 (2006) 091917.
[20] S.-Y. Chung, S.-I. Lee, J.-H. Choi, S.Y. Choi, Appl. Phys. Lett. 89 (2006) 191907.
[21] A.K. Rai, K.D. Mandal, D. Kumar, O. Parkash, J. Alloys Compd. 491 (2010) 507–512.
[22] P. Leret, J.F. Fernandez, J. de Frutos, D.-F. Hevia, J. Eur. Ceram. Soc. 27 (2007) 3901–3905.
[23] H. Xue, X. Guan, R. Yu, Z. Xiong, J. Alloys Compd. 482 (2009) L14–L17.
[24] C. Mu, H. Zhang, Y. He, P. Liu, Physica B 405 (2010) 386–389.
[25] R.D. Shannon, Acta Crystallogr. A 32 (1976) 751–767.
[26] T.H. De Keijser, J.I. Langford, E.J. Mittemeijer, A.B.P. Vogels, J. Appl. Cryst. 15 (1982) 308–314.
[27] G. Deng, N. Xanthopoulos, P. Muralt, Appl. Phys. Lett. 92 (2008) 172909.
[28] Y. Chen, K. Xie, Z.X. Liu, Appl. Surf. Sci. 133 (1998) 221–224.
[29] T. Christmann, B. Felde, W. Niessner, D. Schalch, A. Scharmann, Thin Solid Films 287 (1996) 134–138.
[30] C. Blaauw, F. Leenhouts, F. van der Woude, G.A. Sawatzky, J. Phys. C: Solid State Phys. 8 (1975) 459–468.
[31] E.Z. Kurmaev, V.M. Cherkashenko, Y.M. Yarmoshenko, S. Bartkowski, A.V. Postnikov, M. Neumann, L.C. Duda, J.H. Guo, J. Nordgren, V.A. Perelyaev, W. Reichelt, J. Phys.: Condens. Matter 10 (1998) 4081–4091.
[32] Y. Dachuan, X. Niankan, Z. Jingyu, Z. Xiulin, J. Phys. D: Appl. Phys. 29 (1996) 1051–1057.
[33] Y. Dachuan, X. Niankan, Z. Jingyu, Z. Xiulin, Mater. Res. Bull. 31 (1996) 335–340.
[34] J. Cui, D. Da, W. Jiang, Appl. Surf. Sci. 133 (1998) 225–229.
[35] G. Cao, L. Feng, C. Wang, J. Phys. D: Appl. Phys. 40 (2007) 2899–2905.
[36] L. Marchin, S. Guillemet-Fritsch, B. Durand, A.A. Levchenko, A. Navrotsky, T. Lebey, J. Am. Ceram. Soc. 91 (2) (2008) 485–489.
[37] T.T. Fang, L.-T. Mei, H.F. Ho, Acta Mater. 54 (2006) 2867.
[38] Y.H. Lin, J. Cai, M. Li, C.W. Nan, J. He, J. Appl. Phys. 103 (2008) 074111.
[39] J. Ross Macdonald, Impedance Spectroscopy, Wiley, New York, 1987.
[40] D.R. Clarke, J. Am. Ceram. Soc. 82 (1999) 485–502.
[41] V.P.B. Marques, A. Ries, A.Z. Simoes, M.A. Ramirez, J.A. Varela, E. Longo, Ceram. Int. 33 (2007) 1187–1190.
[42] M.A. Ramírez, P.R. Bueno, Varela S A.-J.A., E. Longo, Appl. Phys. Lett. 89 (2006) 212102.